

Multi-accretion events from corotating and counterrotating SMBHs tori

Daniela Pugliese* and Zdenek Stuchlík

Institute of Physics and Research Centre of Theoretical Physics and Astrophysics, Faculty of Philosophy & Science, Silesian University in Opava, Bezručovo náměstí 13, CZ-74601 Opava, Czech Republic

E-mail: d.pugliese.physics@gmail.com; zdenek.stuchlik@physics.cz

Ringed accretion disks (**RADs**) are aggregates of corotating and counterrotating toroidal accretion disks orbiting a central Kerr super-massive Black Hole (**SMBH**) in **AGNs**. The dimensionless spin of the central **BH** and the fluids relative rotation are proved to strongly affect the **RAD** dynamics. There is evidence of a strict correlation between **SMBH** spin, fluid rotation and magnetic fields in **RADs** formation and evolution. Recently, the model was extended to consider **RADs** constituted by several magnetized accretion tori and the effects of a toroidal magnetic field in **RAD** dynamics have been investigated. The analysis poses constraints on tori formation and emergence of **RADs** instabilities in the phases of accretion onto the central attractor and tori collision emergence. Magnetic fields and fluids rotation are proved to be strongly constrained and influence tori formation and evolution in **RADs**, in dependence on the toroidal magnetic fields parameters. Eventually, the **RAD** frame investigation constraints specific classes of tori that could be observed around some specific **SMBHs** identified by their dimensionless spin

Keywords: Accretion; Accretion disks; Black holes; Active Galactic Nuclei (AGN)

1. Introduction

Ringed accretion disks (**RADs**) are aggregates of axi-symmetric tori orbiting Kerr **SMBHs**. The orbiting agglomerate is composed by both corotating and counterrotating tori. These configurations might be generated after different periods of the attractor life, where the angular momentum of the material in accretion on the central attractor in different phases of the **BH** life could have very different direction and magnitude. The **RAD** model was first developed considering tori centered on the equatorial plane of the central **BH**. **RAD** can be associated to jet emission in many ways, because of the inner edge of accreting disks jet launch point correlation and because the model adopted for each toroidal disk component of the aggregate provides an open solution, proto-jets, consisting of shells funnels of matter along the axis of the **BH**^{2,3,5}. It should be noted that the occurrence of double accretion in the **RAD** is restricted to the case of two tori only, for a couple made by an inner corotating torus and by an outer counterrotating one. Consequently, the double jet shell emission in this system is limited to a jet from external counterrotating matter and an inner jet from the internal corotating matter². It was also provided a general classification of the **RAD** and of the attractors according to their dimensional spin, providing an indication on the configurations and situation where observational evidences can be found. In⁶ a large part of modellization was dedicated to describing the **RAD** as a single disk: in fact it has been shown that such kind of agglomerate is generically a geometrically thin disk, axis-symmetric,

2

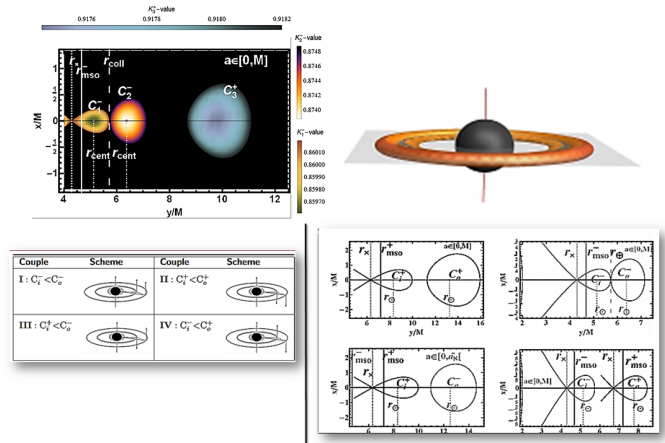


Fig. 1. Upper Left: **RAD** of the order 3, 2D-GRHD density profiles. Upper Right: **RAD** of the order 2, 3D-GRHD density profiles of corotating colliding tori. Below Left: schemes for the ℓ corotating (ℓc) or ℓ counterrotating (ℓr) couples. Below Right: correspondent **RAD** density profiles. Upper line is for the (ℓc) of counterrotating (left) and corotating (right) tori^{1,3}.

with knobby surface, and a very varied internal activity—Figs (1). The **RAD** could be disguised as one disk characterized by articulated phases of super-Eddington accretion, which could explain the masses problem of super-massive **BH** at high redshift, after a series of interrupted phase of accretion^{–1}.

The model was introduced in⁸ and fully developed in⁶. In⁵ the unstable configurations were analyzed and particularly constrains on locations of inner and outer edges of the **RAD** and the toroidal components were given. A detail analysis of **RAD** tori sequences as remnants of multiple accreting periods of Kerr **SMBHs**, in active galactic nuclei (**AGNs**) was considered in³. In⁴, the constraints on double configurations, constituted by two tori centered on the **BH** were given considering the possibility of collision emergence. Energetics associated to the **RAD** processes occurring in the ringed structure between its components and particularly the evaluation of **BH** accretion rates is presented in¹. Here we present the main results of the hydrodynamic (HD) and magnetized **RAD** based on the investigation in^{1,3,7–7}.

Overview In Sec. (2) General considerations on hydrodynamic **RAD** models are discussed. In Sec. (3) constraints are discussed. In Sec. (4) we discuss the effects of toroidal magnetic fields on **RADs**. Concluding remarks follow in Sec. (5).

2. Orbiting Axi-symmetric tori in a Kerr spacetime

Because of the stationarity (time t independence) and the axis-symmetry (ϕ -independence) of each toroid of the aggregate, each torus is regulated by the Euler

equation only with a barotropic equation of state $p = p(\rho)$, there is

$$\int_z^p \frac{dp}{p + \rho} = W(p) - W(0) = -\ln \frac{U_t}{(U_t)_{in}} + \int_{l_{in}}^l \frac{\Omega dl}{1 - \Omega l}, \quad (1)$$

where Ω is the fluid relativistic angular frequency, l specific angular momenta, here assumed constant and conserved inside each torus but not in the **RAD**, (t, r, ϕ, θ) are Boyer-Lindquist (B-L) coordinates. We consider $l > 0$ for *corotating* and $l < 0$ for *counterrotating* fluids, within the notation (\mp) respectively. $a = J/M \in]0, M]$ is the **BH** spin, J is the total angular momentum of the gravitational source and M is the gravitational mass parameter. For the tori couple $(C_{(i)}, C_{(o)})$, orbiting in the equatorial plane of a given Kerr **BH** with specific angular momentum $(\ell_{(i)}, \ell_{(o)})$, we introduce the concept of *lcorotating* (**lc**) disks, defined by the condition $\ell_{(i)}\ell_{(o)} > 0$, and *lcounterrotating* (**lr**) disks defined by the relations $\ell_{(i)}\ell_{(o)} < 0$. The two (**lc**) tori can be both corotating, $la > 0$, or counterrotating, $la < 0$, with respect to the central attractor $a > 0$. Each **RAD** torus is a General Relativistic (GR) model based on the Boyer theory of the equi-pressure surfaces. Boyer surfaces are constant pressure surfaces and $\Sigma_i = \Sigma_j$ for $i, j \in (p, \rho, \ell, \Omega)$. Toroidal surfaces correspond to the equipotential surfaces, critical points of $V_{eff}(\ell)$ as function of r , thus solutions of $W : \ln(V_{eff}) = c = \text{constant}$ or $V_{eff} = K = \text{constant}$ **C**-cross sections of the closed Boyer surfaces (equilibrium quiescent torus); **C_x**-cross sections of the closed cusped Boyer surfaces (accreting torus); **O_x**-cross sections of the open cusped Boyer surfaces, generally associated to proto-jet configurations. In the following we use the notation $()$ to indicate a configuration which can be closed, **C**, or open **O**-Figs (1). The model is constructed investigating the angular momentum distribution inside the disk (which is not constant):

$$\pm \ell_n^\mp = \pm \frac{a^3 + ar_n(3r_n - 4M) \mp \sqrt{r_n^3 \Delta_n^2}}{a^2 - (r_n - 2M)^2 r_n} \Big|_{r_n^*}, \quad \Delta_n \equiv r_n^2 - 2Mr_n + a^2 \quad (2)$$

where n is for the toroidal **RAD** component, and Δ_n is here a metric factor. In fact an essential part of the **RAD** analysis is the characterization of the boundary conditions on each torus in the agglomerate and of the disk. We considered also the function

$$K^\pm(\Delta_{(\pm)}, r) \equiv \frac{1}{2} \sqrt{\frac{r[(\Delta_- - \Delta_+)^2 + 4(r-2)r]}{2\Delta_-^2 - \Delta_- \Delta_+ r + r^3}} \Big|_{\tilde{r}_n^\mp}, \quad \ell = \frac{\Delta_- + \Delta_+}{2}, \quad a = \frac{(\Delta_+ - \Delta_-)}{2} \quad (3)$$

(dimensionless units), provides constrains on the matter density distribution inside the disk and stitching together the **RAD** tori.

3. Constraints

In the Bondi quasi spherical accretion, the fluid angular momentum is everywhere smaller than the Keplerian one and therefore dynamically unimportant. In this analysis, however, we consider a full GR model for each **RAD** toroid where in fact

4

there exists an extended region where the fluids angular momentum in the torus is larger (in magnitude) than the Keplerian (test particle) angular momentum. More precisely as first canvas model we adopt for each toroid a thick, opaque (high optical depth) and super-Eddington, radiation pressure supported accretion disk (in the toroidal disks, pressure gradients are crucial) cooled by advection with low viscosity. As a consequence, during the evolution of dynamical processes, the functional form of the angular momentum and entropy distribution depends on the initial conditions of the system and on the details of the dissipative processes. From these considerations, using the distribution of relativistic specific angular momentum in the **RAD** as in Eq. (2) we can fix, as in^{1,4-6}, the constraints on the range of variation of the inner edge of accreting torus, r_x , and on the point of maximum density (pressure) in each torus, r_{cent} , in dependence from the range of variation of the specific angular momentum in the disk. Precisely, constraints on the angular momentum ℓ ranges are as follow:

[Range- L1] $\mp \mathbf{L1}^\pm \equiv [\mp \ell_{mso}^\pm, \mp \ell_{mbo}^\pm[$ where topologies (C_1, C_\times) are possible, with accretion point in $r_\times \in]r_{mbo}, r_{mso}]$ and center with maximum pressure $r_{cent} \in]r_{mso}, \rho_{mbo}]$;
[Range- L2] $\mp \mathbf{L2}^\pm \equiv [\mp \ell_{mbo}^\pm, \mp \ell_\gamma^\pm[$ where topologies (C_2, O_\times) are possible, with unstable point $r_j \in]r_\gamma, r_{mbo}]$ and center with maximum pressure $r_{cent} \in]\rho_{mbo}, \rho_\gamma]$;
[Range- L3] $\mp \mathbf{L3}^\pm \equiv \ell \geq \mp \ell_\gamma^\pm$ where only equilibrium torus C_3 is possible with center $r_{cent} > \rho_\gamma$; (in the following indices $i \in \{1, 2, 3\}$ refer to the ranges of angular momentum $\ell \in \mathbf{Li}$ being mso =marginally stable orbit and mbo =marginally bounded orbit, γ =marginally circular orbit (photon orbit.) Alongside the geodesic structure of the Kerr spacetime represented by the set of radii $R \equiv (r_{mso}^\pm, r_{mbo}^\pm, r_\gamma^\pm)$, and $r_{\mathcal{M}}^\pm$ solution of $\partial_r^2 \ell = 0$, relevant to the location of the disk center and outer edge are $R_\rho \equiv (\rho_{mbo}^\pm, \rho_\gamma^\pm, \rho_{\mathcal{M}}^\pm) ::$

$$\begin{aligned} r_\gamma^\pm < r_{mbo}^\pm < r_{mso}^\pm < \rho_{mbo}^\pm < \rho_\gamma^\pm \quad \text{where} \quad \rho_{mbo}^\pm : \ell_\pm(r_{mbo}^\pm) = \ell_\pm(\rho_{mbo}^\pm) \equiv \ell_{\mathbf{mbo}}^\pm, \\ \rho_\gamma^\pm : \ell_\pm(r_\gamma^\pm) = \ell_\pm(\rho_\gamma^\pm) \equiv \ell_\gamma^\pm, \quad \rho_{\mathcal{M}}^\pm : \ell_\pm(\rho_{\mathcal{M}}^\pm) = \ell_{\mathcal{M}}^\pm. \end{aligned} \quad (4)$$

This expanded structure rules good part of the geometrically thick disk physics and multiple structures. The presence of these radii stands as one of the main effects of the presence of a strong curvature of the background geometry^{1,3,5}.

3.1. The **RAD** constraints

The **RAD** of the order $n = 2$ (the order n is the number of toroidal components) can be composed by the the following toridal couples:

i) $C_\times^\pm < C^\pm$, **ii)** $C_\times^+ < C^\pm$, **iii)** $C_\times^- < C^\pm$ and **iv)** $C_\times^- < C_\times^+$. We indicated with $<$ the relative rotation of maximum density points in the tori—Figs (1). The situation concerning the emergence of more accretion points in **RAD** and presence of double accretion and screening tori, is summarized as follows:

$$\text{for } a \in]0, M[: \quad \underbrace{C_\times^-}_{(a)} < \dots < C_- < \dots < \underbrace{C_\times^+}_{(c)} < \dots < \underbrace{C_\pm}_{(d)} < \dots \quad (5)$$

where (a) is the inner ring in accretion, (b) is the inner subsequence of corotating tori in equilibrium, (c) is the outer accreting tori and (d) is the outer (mixed or separated) subsequence composed by equilibrium tori only. Further constraints (for the specific angular momentum, elongation and number n of tori) on the subsequences (b) and (d) depend on the attractor spin mass ratio—Figs (1). More precisely:

The RAD canvas

- There is a maximum $n = 2$ of accreting tori of the kind $C_x^- < C_x^+$ around supermassive BHs with $a \neq 0$. Such tori are strongly constrained in their values of ℓ and K depending on the spin-mass ratio of the attractor.

- “Screening”-tori located between the accreting disk and the central BH in a RAD sequence as $C_x^- < C^- < \dots < C_x^+ < C^\pm$ are possible only as corotating, quiescent C^- inner tori. A screening torus is a corotating (non-accreting) torus eventually detectable by X-ray spectra emission obscuration.

- If a counterrotating torus of a RAD is accreting onto the central BH, then a RAD with a corotating outer C_1^- torus, is as $(\)^- < C_x^+ < C_1^- < C^\pm$, only orbiting “slow” SMBHs ($a < 0.46M$).

[-Corotating Tori] A corotating torus can be the outer of a couple with an inner counterrotating accreting torus. Then the outer torus may be corotating (non accreting), or counterrotating in accretion or quiescent. Both the inner corotating and the outer counterrotating torus of the couple can accrete onto the attractor.

[-Counterrotating Tori] A counterrotating torus can therefore reach the instability being the inner of a (ℓr)-(ℓc), or the outer torus of a (ℓr) couple. If the accreting torus is counterrotating, C_x^+ , with respect to the Kerr attractor, there is no inner counterrotating torus, but there is $C_x^+ < C^\pm$ or $(\)^- < C_x^+$.

4. Influence of toroidal magnetic field in multi-accreting tori

We considered a toroidal magnetic field contribution in each RAD component where the magnetic field is⁻⁹:

$$B^\phi = \sqrt{\frac{2p_B}{g_{\phi\phi} + 2\ell g_{t\phi} + \ell^2 g_{tt}}} \quad \text{with} \quad p_B = \mathcal{M} (g_{t\phi} g_{t\phi} - g_{tt} g_{\phi\phi})^{q-1} \omega^q \quad (6)$$

the magnetic pressure, ω is the fluid enthalpy, q and \mathcal{M} (magnitude) are constant; V_{eff} is a function of the metric and the angular momentum ℓ . Euler equation (1) is modified by the term:

$$\partial_\mu \tilde{W} = \partial_\mu [\ln V_{eff} + \mathcal{G}] \quad \mathcal{G}(r, \theta) = \mathcal{S} (g_{t\phi} g_{t\phi} - g_{tt} g_{\phi\phi})^{q-1}, \quad \mathcal{S} \equiv \frac{q \mathcal{M} \omega^{q-1}}{q-1}, \quad (7)$$

(where $a \neq 0$) $q = 1$, is a singular values for the magnetic parameter \mathcal{S} , which is negative at $q < 1$, in this case excretion tori are possible. We here concentrate on $q > 1$. We therefore consider the equation for the $\tilde{W} = K$. For $\mathcal{S} = 0$ (or $\mathcal{M} = 0$) this reduces to the HD case. The RAD angular momentum distribution is:

$$\tilde{\ell}^\mp \equiv \frac{a^3 + ar [4\mathcal{Q}(r-M)\mathcal{S}\Delta^\mathcal{Q} + 3r-4] \mp \sqrt{r^3\Delta^2 [1 + [2\mathcal{Q}(r-1)^2 r \mathcal{S} \Delta^{\mathcal{Q}-1} (2\mathcal{Q}\mathcal{S}\Delta^\mathcal{Q} + 1)]}}{\Delta^{-1} [a^4 - a^2(r-3)(r-2)r - (r-2)r [2\mathcal{Q}(r-1)\mathcal{S}\Delta^{\mathcal{Q}+1} + (r-2)^2 r]]} \quad (8)$$

6

$Q \equiv q - 1$ (dimensionless units). However the introduction of a toroidal magnetic field B , makes the study of the momentum distribution within the disk rather complicated, instead In⁷ it was adopted the function derived from **S-RAD** parameter:

$$\mathcal{S}_{crit} \equiv -\frac{\Delta^{-Q} a^2(a-\ell)^2 + 2r^2(a-\ell)(a-2\ell) - 4r(a-\ell)^2 - \ell^2 r^3 + r^4}{Q} \frac{1}{2r(r-1)[r(a^2-\ell^2) + 2(a-\ell)^2 + r^3]} \quad (9)$$

(dimensionless units) capable of setting the location of maximum density points in the disk and the existence and location of the instability points. Eq. (9) clearly enunciates the magnetic field contribution in the Q term, while interestingly highlights the role of the parameters ℓ versus $a^{-2,8}$. The effects of the toroidal magnetic field in the **RAD** composition are evident in Fig. (2). In⁷ it is noted that a **RAD** can be formed by having generally a sufficiently small parameter ($\mathcal{S}q$). Profiles of (ℓc) cases are similar independently by the corotation or counterrotation of the fluids in the **RAD** with the respect to the central Kerr **SMBH**. Generally the inner torus has maximum values of the \mathcal{S} smaller the maximum \mathcal{S} found in the outer tori. The most interesting results perhaps emerge in the case of (ℓr) couples where it is clear that the magnetic profiles for the couple $C_- < C_+$ (where double accretion occurs) are radically different from the case $C_+ < C_-$. The analysis shows also the importance of the coupling between the toroidal component of the magnetic field and the fluid angular momentum, particularly in the counter-rotating case, $\ell < 0$; for this case, for values $q < 1$ excretion can arise⁷⁻¹⁰.

Effects of toroidal magnetic fields on RADs

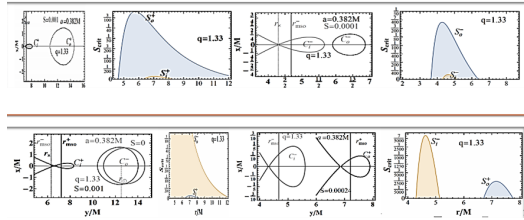


Fig. 2. Magnetized **RAD** of the order $n = 2$. Density profiles versus \mathcal{S} functions profiles. Upper line features the ℓ corotating couples of corotating (-) and counterrotating (+) tori. Bottom line features the ℓ counterrotating couples made by $C_+ < C_-$ (left) or $C_- < C_+$ (right). From⁷.

5. Concluding Remarks and Future perspectives

The **RAD** investigation has revealed a very rich scenario with interesting phenomenology linked to the activity inside the agglomeration, correlated to the processes of instability and interaction between tori and the tori and central **SMBH** attractor. In this scenario constraints on the presence of screening and obscuring tori were discussed. The analysis of the screening and obscuring tori in particular could lead to observational evidences of a double tori **RAD** system from the emission

spectrum as X-ray emission screening, showing as fingerprints of the discrete radial profile of the **RAD**. In¹¹ then relatively indistinct excesses of the relativistically broadened emission-line components were predicted arising in a well-confined radial distance in the accretion structure originating by a series of episodic accretion events. Another interesting aspect of this model is the possibility of having inter-disk activity resolved in tori collision or double accretion phase with a double jet emission phase. From the **RAD** investigation this activity is limited to only two specific tori of aggregate made by a special couple constituted by a corotating and a counterrotating torus. As sideline result we provided a full characterization of the counterrotating tori in the multi-accreting systems. This model is designed for an extension to a dynamic GRMHD setup. Currently the toroidal model adopted to picture each **RAD** components is used as initial configuration for such systems. Another significant aspect is the possibility of inter-correlate the oscillations of the **RAD** components with **QPOs**. Generally instabilities of such configurations, can reveal to be of great significance for the High Energy Astrophysics related to accretion onto supermassive **BHs**, in Quasars and **AGNs**. Such activities could be targeted by the planned X-ray observatory **ATHENA**^a.

Acknowledgments

D.P. acknowledges support from the Junior GACR grant of the Czech Science Foundation No:16-03564Y.

References

1. D. Pugliese and Z. Stuchlik, *Class. Quant. Grav.* **35**, 18, 185008 (2018).
2. D. Pugliese and Z. Stuchlik, *Class. Quant. Grav.* **35**, 10, 105005 (2018).
3. D. Pugliese, & Z. Stuchlík, *JHEAp* **17** 1-37, (2018).
4. D. Pugliese, &Z. Stuchlík, *APJS* **229** 2, 40, (2017).
5. D. Pugliese, &Z. Stuchlík, *APJS*, **223**, 2, 27, (2016).
6. D. Pugliese Z. &Z. Stuchlík, *APJS*, **221** 25 (2015).
7. D. Pugliese &G. Montani, *MNRAS*, **476**, 4, P4346-4361 (2018).
8. D. Pugliese, & G. Montani, *Phys.Rev. D* **91**, 8, 083011 (2015).
9. S. S. Komissarov, *MNRAS*, **368**, 993 (2006); K. Adamek & Z. Stuchlik, *Class. Quantum Grav.* **30**, 205007 (2013).; D. Pugliese &G. Montani, *EPL*, **101**, 1, 19001 (2013).
10. Z. Stuchlik, P. Slany, J. Kovar, *Class. Quantum Grav.*, **26**, 215013 (2009).
11. V. Sochora, V. Karas, et al., *MNRAS*, **418**, 276-283 (2011) ; J. Schee &Z. Stuchlik, *Gen. Rel. Grav.*, **41**, 1795 (2009). ;J. Schee &Z. Stuchlik, *JCAP*, **1304**, 005 (2013).

^a<http://the-athena-x-ray-observatory.eu/>